

PLANNING AND CONTROL OF AGGRESSIVE MANEUVERS FOR PERCHING ON INCLINED AND VERTICAL SURFACES

Justin Thomas*

GRASP Lab

MEAM[†]

University of Pennsylvania
Philadelphia, Pennsylvania 19104
jut@seas.upenn.edu

Giuseppe Loiano

GRASP Lab

MEAM[†]

University of Pennsylvania
Philadelphia, Pennsylvania 19104
loianog@seas.upenn.edu

Morgan Pope

Elliot W. Hawkes

Matthew A. Estrada

Hao Jiang

Mark R. Cutkosky

Department of Mechanical Engineering
Stanford University
Stanford, California 94305

{mpope, estrada1, jianghao, cutkosky}@stanford.edu

Vijay Kumar

GRASP Lab

MEAM[†]

University of Pennsylvania
Philadelphia, Pennsylvania 19104
kumar@seas.upenn.edu

ABSTRACT

It is important to enable micro aerial vehicles to land and perch on different surfaces to save energy by cutting power to motors and to perform tasks such as persistent surveillance. In many cases, the best available surfaces may be vertical windows, walls, or inclined roof tops. In this paper, we present approaches and algorithms for aggressive maneuvering to enable perching of underactuated quadrotors on surfaces that are not horizontal. We show the design of a custom foot/gripper for perching on smooth surfaces. Then, we present control and planning algorithms for maneuvering to land on specified surfaces while satisfying constraints on actuation and sensing. Experimental results that include successful perching on vertical, glass surfaces validate the proposed techniques.

INTRODUCTION

Micro Aerial Vehicles (MAVs) have become ubiquitous, but they suffer from limited energy density batteries, which restricts

their mission time [1]. Many tasks, however, do not require the robot to be in motion. In fact, some tasks do not even require the robot to be airborne. For example, a robot may be tasked with the objective to monitor a crime scene until police arrive or to monitor the gas levels of a nearby gas leak. In such cases, the vehicle could not only be stationary, but could also perch and turn off its motors to preserve energy for the next task. Perching capabilities could also be useful for tasks which require the robot to maintain a precise, static position, act as a radio relay in disaster zones, or to suspend operation during a period of unfavorable weather. Thus, perching is an appealing capability for aerial vehicles.

Fixed wing vehicles are appealing because they typically have longer flight times than rotorcraft, but they cannot as easily hover in place. Multiple works leverage penetration-based grasping to perch using fixed-wing aircraft on vertical walls [2, 3, 4]. Other results enable perching on cables such as power lines [5, 6]. However, detecting cables and performing relative pose estimation using onboard sensors and computation in real-time, real-world, scenarios would make such approaches very difficult in practice for fast-moving, micro-sized fixed-wing aircraft.

Quadrotors, on the other hand, can carry larger payloads

*Address all correspondence to this author.

[†]Department of Mechanical Engineering and Applied Mechanics

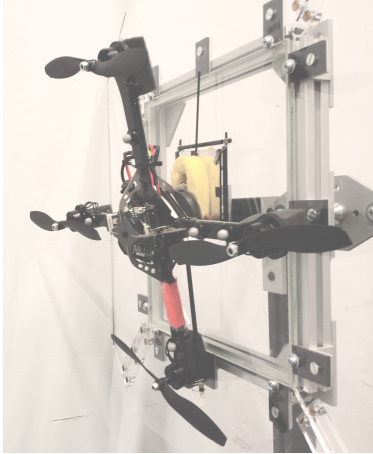


FIGURE 1. A quadrotor perched on a vertical glass surface.

for their size (*i.e.* more processing power and sensors per footprint) and can provide both slow and fast, agile movements, which makes them useful in many scenarios. Their flight time is more restricted, which makes the motivation for perching even stronger. A bioinspired, passive perching mechanism was developed in [7] and [8], but the mechanism was too heavy and was restricted to objects that are narrow enough for the gripper to wrap around. Similarly, [9] presents a gripper that requires cylindrical objects and would restrict the set of possible perch locations based on the size of the gripper. Dry adhesives are used to adhere to flat surfaces in [10], but a planning or control strategy for the robot to achieve perching is not presented. The authors in [11] also use a dry adhesive, but they place the gripper on the side of the robot, requiring extra compensation for the added moment and rendering the gripper only useful for perching tasks. An opposed-grip dry adhesive is used in [12] to increase the capable load, but the work focuses on the design of the gripper and uses a launcher to simulate a perching maneuver.

There have also been perching approaches that focus on planning. In [13], a bioinspired trajectory generation method (tau theory) is used for perching, but it does not consider the dynamics or underactuation of the robot, and it only provides kinematic simulations. The authors of [14] and [15] present perching on vertical surfaces, but the gripper uses a hook and loop fastener for adhesion, which is not likely an option in real-world scenarios. Furthermore, they rely on switching between linear controllers as well as iterative learning for successful perching. Their work is extended in [16] where time constants for attitude commands are incorporated, but the system still uses a state machine to toggle between a trajectory and attitude controller. All sensing and processing is conducted onboard the robot in [17], but once again, the perching uses a hook and loop fastener.

In our previous work, a robot was able to grasp objects while the robot was in motion, and the extension to perching would be

straightforward [18]. However, the gripper was quite massive relative to the size of the robot and impacted the dynamics of the overall system, motivating its consideration when planning aggressive trajectories for grasping. Further, possible perch locations are limited to horizontal flat surfaces or small enough cylinders. Since an aerial robot would most often be observing things below, it is desirable to avoid perching on flat surfaces since they would interfere with downwards observations.

In this work, we present a method that incorporates both a downwards-facing, real-world gripping mechanism as well as a control and planning strategy for quadrotors to achieve the necessary conditions for perching on smooth, vertical surfaces (see Figure 1). A passively actuated, downwards-facing, dry-adhesive gripper is presented and used to adhere to such surfaces, and its requirements for successful perching (*i.e.* its *landing envelope*) are explored. The downwards-facing gripper motivates a strategic approach for trajectory planning since the system is under-actuated such that the orientation and the position of the robot cannot be simultaneously controlled. Thus, we present a suitable method for trajectory generation, which considers actuator and sensor constraints to ensure that the planned trajectories are not only dynamically feasible, but also realizable on the physical platform, and ensure that the robot perches within the landing envelope of the gripper. Finally, we present experiments using a quadrotor equipped with the proposed gripper.

The key contributions of this paper are threefold: (1) We design and characterize a passively-actuated, opposed-grip, dry adhesive, gripper for use on an MAV. (2) We present a method for control and planning to ensure that the robot’s perch will fall within the landing envelope. (3) Experimental results demonstrate the effectiveness of the gripper, controller, and the planning strategy.

The rest of the paper is organized as follows: First, we provide an overview of the design of the gripper and explore the landing envelope of the gripper. Following the gripper design, the dynamics and controller for the robot are presented. Then, the method for planning physically realizable trajectories considering actuator and sensor constraints is developed. Finally, experimental results are demonstrated and we conclude the paper, offering a path for continued development.

A GECKO INSPIRED GRIPPER

We present a gripper that is gecko-inspired in the sense that it uses thin, compliant wedges, similar to geckos’ feet, that dramatically change their contact area with a surface in response to shear loads. The laying down of these “micro-wedges” generates normal adhesion due to van der Waals forces. The adhesive is lightweight (only 12 grams of adhesive tile are needed for this application) and enables perching on smooth surfaces. In the rest of this section, we will first explain the mechanical design of the gripper and then push its capabilities by exploring the landing

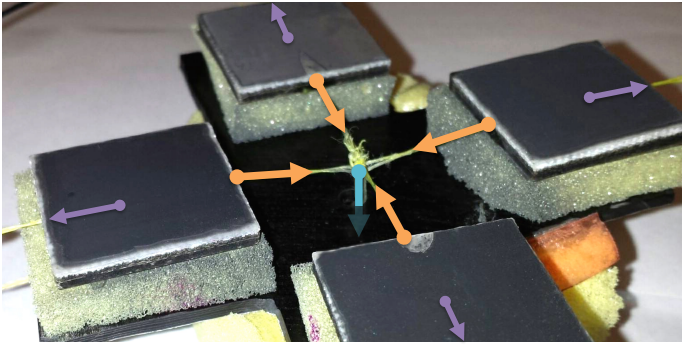


FIGURE 2. A view of the underside of the gripper. Initially, the pads are held in place by slight tension between the purple and orange arrows (opposed). Then, upon collapse of the truss mechanism, each pad is placed in shear by pulling the pad towards the center (orange arrows) of the gripper using the tension string (blue downwards arrow).

envelope.

Mechanical Design

The gripper has four pads, each of which is a directional adhesive. When placed in shear, the pads adhere to the surface by increasing the contact area, and thereby increasing the sustainable normal force. Arranged in a “plus” configuration, the opposing pads provide the necessary balance to create shear while allowing a significant normal force (see Figure 2). The gripper is not sticky to the touch, and hence is referred to as a “dry” adhesive. In this work, the gripper configuration was modified and scaled up for use on a larger vehicle than used in [10] and [12].

Ground effects and the reduction in control authority during an aggressive pitching maneuver both favor a relatively high incoming velocity for the quadrotor, which in turn effects the loading strategy and the suspension between the gripper and the quadrotor. The high incoming velocity and the high stiffness of both the quadrotor and the landing surface means that the robot is only in contact with the wall for a short amount of time and that the rebound can be quite violent. The dry adhesives used in the gripper are suited to these applications because they have very short engagement times, which can be further reduced with an effective loading strategy. In the current design, this is achieved by collapsing a bi-stable truss mechanism when the gripper impacts the wall, instantly transmitting a high shear force to the pads while they are still pressed against the surface. When loaded in high shear while in compression, the adhesive can achieve full attachment strength in less than ten milliseconds.

To reduce the violence of rebound and give the robot the maximum amount of time possible on the wall, damping foam is employed to absorb some of the impact energy. To limit the peak

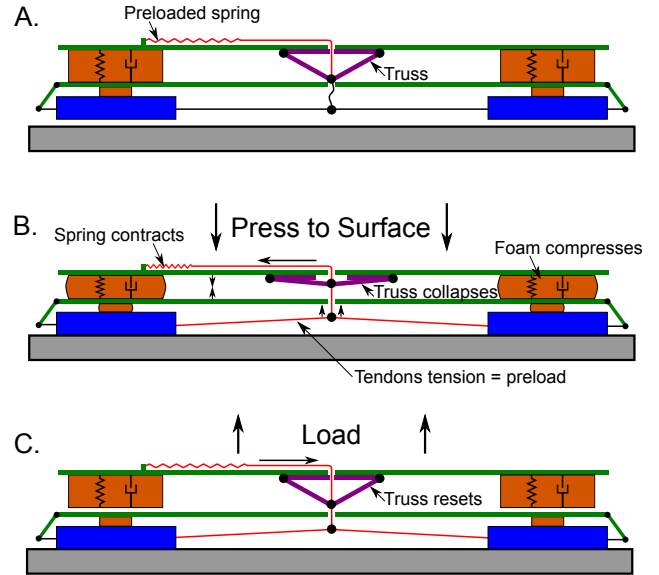


FIGURE 3. A cross-section view of the gripper. The bistable truss mechanism is used to engage the directional adhesive pads upon contact with the surface. (A) Initially, a preloaded spring is tensioned low enough that the truss does not collapse. (B) Upon an impact, the truss collapses (the magnets holding the one side together separate) and the tension in the spring is transmitted via tendons to the gripping pads to create shear. (C) When the robot creates tension in the tendon, whether from the rebound or from static hanging, the truss mechanism resets, and the tension remains transmitted to the pads since the entire mechanism is being pulled away.

forces experienced by the gripper, a spring element is the only mechanical connection between the gripper and the quadrotor. It consists of a soft, linear spring which is pre-loaded to support the robot’s weight when unextended and to give several centimeters of deflection before approaching the gripper’s adhesive limit, thus maximizing energy absorption during rebound. The combination of effective loading strategy as well as energy dissipation and absorption enables the robot to successfully perch at velocities as high as 2 m/s.

A schematic of the mechanism is presented in Figure 3 and a picture with arrows indicating the tensioning directions is provided in Figure 2. With a mass of only 70 grams, the mechanism is very lightweight and promises to provide more benefit for perching than the cost of the additional payload. The utility of the final design can be described by the range of impact conditions which result in secure attachment to the wall. A boundary inside of which perching is expected to succeed is referred to as a landing envelope, and it is important for understanding the robustness of the mechanical design.

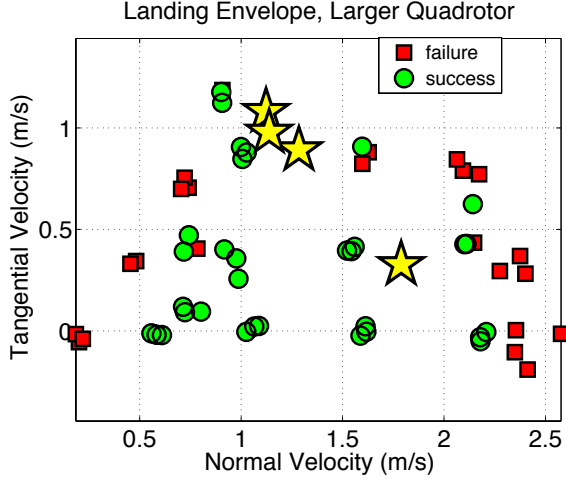


FIGURE 4. The results from the landing envelope of the gripper and quadrotor system. The successful perches are shown in green circles and the failures are the red squares when launched onto the perch location. Yellow stars indicate successes for trials while the quadrotor was flying. One can observe that the ideal normal velocity is about 1.2 m/s with a maximum allowable tangential velocity of around 1.1 m/s.

The Landing Envelope

The landing envelope of the gripper is determined experimentally by launching the robot towards a smooth glass surface at varying normal and tangential velocities. The velocities are estimated using a high speed camera with successful and unsuccessful perches recorded in Figure 4. The results indicate that a minimum normal velocity is desired (to properly align the pads and engage the collapsing truss mechanism), a maximum normal velocity must be avoided (to prevent bottoming out the suspension spring element), and that the addition of velocity tangential to the wall can be tolerated only up to a certain point (when the kinetic energy again becomes too great for the suspension to dissipate). In active flight, the control strategy described in the rest of this paper is able to create landing conditions which meet these requirements, resulting in successful perching (plotted as yellow stars in Figure 4).

DYNAMICS AND CONTROL

In this work, the robot used is a quadrotor, which is a multi-rotor vehicle consisting of four rotors with parallel axes of rotation as displayed in Figure 5. The rest of this section will present the dynamics of the system followed by a control law.

Preliminaries and Dynamics

The speed of the rotors, ω_i , can be mapped to what we will consider the control inputs for the system using the following

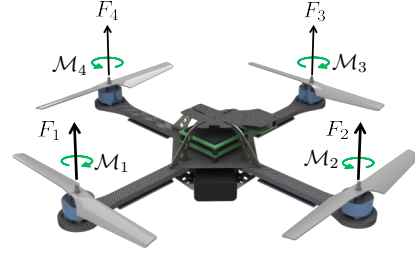


FIGURE 5. A quadrotor has four rotating propellers. Each rotor generates a force, F_i , and a moment, M_i . Adjacent rotors spin the opposite direction so that the moment resulting from drag is opposing and can be controlled by varying the speed of the pairs of rotors.

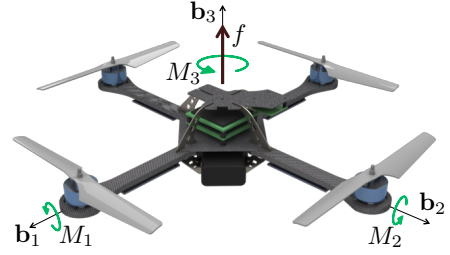


FIGURE 6. The control inputs of a quadrotor can be considered to be a net force, f , and moments about each of the principal axes, M_i .

invertible transformation

$$\begin{bmatrix} f \\ M_1 \\ M_2 \\ M_3 \end{bmatrix} = \begin{bmatrix} k_f & k_f & k_f & k_f \\ 0 & lk_f & 0 & -lk_f \\ -lk_f & 0 & lk_f & 0 \\ k_m & -k_m & k_m & -k_m \end{bmatrix} \begin{bmatrix} \omega_1^2 \\ \omega_2^2 \\ \omega_3^2 \\ \omega_4^2 \end{bmatrix} \quad (1)$$

where k_f and k_m are the thrust and moment coefficients of the rotors, respectively, and the distance between the axis of rotation and the center of mass is l . The net thrust is f and the moment about the i^{th} body frame axis is given by M_i . Using this relationship, the system can be treated as having the control inputs as pictured in Figure 6.

Then, the translational dynamics are

$$m\ddot{\mathbf{x}} = fR\mathbf{e}_3 - mg\mathbf{e}_3 \quad (2)$$

where $m \in \mathbb{R}$ is the mass of the vehicle and $\mathbf{x} \in \mathbb{R}^3$ is the position of the robot in the world frame, \mathcal{W} . The rotation from the body frame (\mathcal{B}) to the world frame (\mathcal{W}) is given by $R \in \text{SO}(3)$, g is gravitational acceleration, and \mathbf{e}_3 is the third standard basis vector, $\mathbf{e}_3 = [0 \ 0 \ 1]^T$. The angular dynamics of the system are given by

$$J\dot{\Omega} = \mathbf{M} - \Omega \times J\Omega \quad (3)$$

where $J \in \mathbb{R}^{3 \times 3}$ is the inertia tensor aligned with \mathcal{B} , $\Omega \in \mathbb{R}^3$ is the angular velocity of the vehicle expressed in \mathcal{B} , and $\mathbf{M} = [M_1 \ M_2 \ M_3]^T$ contains the control moments. Equations (3) and (2) are related through the orientation of the robot, namely,

$$\dot{R} = R\hat{\Omega} \quad (4)$$

where $\hat{\cdot} : \mathbb{R}^3 \mapsto \mathfrak{so}(3)$ is the ‘‘hat’’ map and is defined such that if $\mathbf{a}, \mathbf{b} \in \mathbb{R}^3$, $\mathbf{a} \times \mathbf{b} = \hat{\mathbf{a}}\mathbf{b}$.

The Control Law

We implement the control law developed in [19], which guarantees exponential stability if the geodesic attitude error is less than 90° and exhibits almost global exponential attractiveness (the only exception is when the geodesic attitude error is 180°). Let the thrust be

$$f = (-k_x \mathbf{e}_x - k_v \mathbf{e}_v + m \mathbf{g} \mathbf{e}_3 + m \ddot{\mathbf{x}}_d) \cdot \mathbf{R} \mathbf{e}_3 \equiv \mathbf{f}_{des} \cdot \mathbf{R} \mathbf{e}_3 \quad (5)$$

where k_x and k_v are positive gains,

$$\mathbf{e}_x = \mathbf{x} - \mathbf{x}_d \quad \text{and} \quad \mathbf{e}_v = \dot{\mathbf{x}} - \dot{\mathbf{x}}_d$$

are position and velocity errors, respectively, and $\ddot{\mathbf{x}}_d$ is the nominal acceleration. The commanded moments are given by

$$\mathbf{M} = -k_R \mathbf{e}_R - k_\Omega \mathbf{e}_\Omega + \Omega \times J \Omega - J (\hat{\Omega} R^T R_c \Omega_c - R^T R_c \dot{\Omega}_c) \quad (6)$$

where k_R and k_Ω are positive gains and

$$\mathbf{e}_R = \frac{1}{2} (R_c^T R - R^T R_c)^\vee \quad \text{and} \quad \mathbf{e}_\Omega = \Omega - R^T R_c \Omega_c$$

are the angular position and rate errors with $\cdot^\vee : \mathfrak{so}(3) \mapsto \mathbb{R}^3$ being the opposite of the ‘‘hat’’ map. In this case, R_c is considered to be the ‘‘commanded attitude’’, which is given by

$$R_c = [\mathbf{b}_{1_c}, \mathbf{b}_{3_c} \times \mathbf{b}_{1_c}, \mathbf{b}_{3_c}] \quad (7)$$

where

$$\mathbf{b}_{3_c} = \frac{-k_x \mathbf{e}_x - k_v \mathbf{e}_v - m \mathbf{g} \mathbf{e}_3 + m \ddot{\mathbf{x}}_d}{\| -k_x \mathbf{e}_x - k_v \mathbf{e}_v - m \mathbf{g} \mathbf{e}_3 + m \ddot{\mathbf{x}}_d \|} \quad (8)$$

and \mathbf{b}_{1_c} is chosen such that $\mathbf{b}_{3_c} \times \mathbf{b}_{1_c}$ is well conditioned. In our case, it is defined by a combination of the planned trajectory and the desired force and will be explained further in the next section.

PLANNING WITH CONSTRAINTS

The system is underactuated since the control inputs can only directly affect the translational acceleration in the \mathbf{b}_3 direction. Since we are interested in aggressive maneuvers in which the quadrotor can perch on vertical surfaces, it is important to ensure that we can plan trajectories that are not only dynamically feasible (considering the underactuation), but also physically realizable (considering actuator and sensor constraints). We will first explore the dynamic feasibility of a trajectory by presenting a planning method that, by design, can guarantee that a trajectory is dynamically feasible.

Planning for Dynamic Feasibility

In this subsection, we will present results similar to [20], which facilitates the computation of trajectories for the underactuated quadrotor system. We propose the following set of variables called *flat outputs*, which will be used to show that the dynamics of the system can be written in terms of this subset of variables and their derivatives:

$$\mathcal{Y} = [\mathbf{x}^T, \psi]. \quad (9)$$

In fact, the results will demonstrate that the variables are decoupled so that the system can be expressed as a chain of integrators independently in each of the *flat outputs*. This property of the system is called *differential flatness*, and is useful for planning trajectories of underactuated systems [21, 22].

First, observe from (2) that the force can be determined from the acceleration of the trajectory, $\ddot{\mathbf{x}}$, since $\|\mathbf{R} \mathbf{e}_3\| = 1$

$$f = m \|\ddot{\mathbf{x}} + \mathbf{g} \mathbf{e}_3\| \quad (10)$$

and the orientation of the third body frame axis is

$$\mathbf{R} \mathbf{e}_3 = \mathbf{b}_3 = \frac{\ddot{\mathbf{x}} + \mathbf{g} \mathbf{e}_3}{\|\ddot{\mathbf{x}} + \mathbf{g} \mathbf{e}_3\|}. \quad (11)$$

The rest of the rotation matrix, R , can be determined by defining a vector, \mathbf{b}_1 orthogonal to \mathbf{b}_3 using ψ and then using $\mathbf{b}_3 \times \mathbf{b}_1$ to determine \mathbf{b}_2 . In [20], an intermediate vector was defined as $\mathbf{b}_c = [\cos \psi, \sin \psi, 0]$ so that \mathbf{b}_2 could be determined by

$$\mathbf{b}_2 = \frac{\mathbf{b}_3 \times \mathbf{b}_c}{\|\mathbf{b}_3 \times \mathbf{b}_c\|}. \quad (12)$$

However, in our case, such an approach is dangerously close to the singularity that results when \mathbf{b}_3 is parallel to \mathbf{b}_c , which is likely to be the case when perching on a vertical surface since

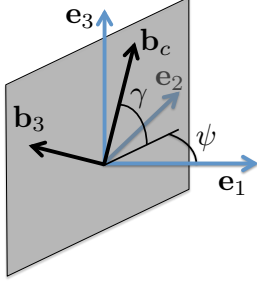


FIGURE 7. We define the \mathbf{b}_c vector based on ψ and \mathbf{b}_3 in order to determine \mathbf{b}_2 while avoiding the singularity when $\mathbf{e}_3 \cdot \mathbf{b}_3 = 0$. This is manifested in the planning, but is used primarily in the control law.

the thrust vector may be horizontal. To avoid this, we choose \mathbf{b}_c such that the singularity is avoided by allowing \mathbf{b}_c to be rotated (no more than $\pm\pi/2$) while remaining in the plane defined by $[\cos \psi, \sin \psi, 0] \times \mathbf{e}_3$. In practice, this means that we can define \mathbf{b}_c as

$$\mathbf{b}_c = \begin{bmatrix} \cos \gamma \cos \psi \\ \cos \gamma \sin \psi \\ \sin \gamma \end{bmatrix}, \quad \gamma \in (-\pi, \pi) \quad (13)$$

where γ is chosen based on \mathbf{b}_3 (see Figure 7). Then, \mathbf{b}_2 is given by (12),

$$\mathbf{b}_1 = \mathbf{b}_2 \times \mathbf{b}_3 \quad (14)$$

and

$$R = [\mathbf{b}_1, \mathbf{b}_2, \mathbf{b}_3]. \quad (15)$$

The next derivative of (2) is given by

$$\begin{aligned} m\mathbf{x}^{(3)} &= f\dot{R}\mathbf{e}_3 + \dot{f}R\mathbf{e}_3 \\ &= fR\hat{\Omega}\mathbf{e}_3 + \dot{f}\mathbf{b}_3 \end{aligned} \quad (16)$$

and the scalar projection onto \mathbf{b}_3 reveals that

$$\dot{f} = \mathbf{b}_3 \cdot m\mathbf{x}^{(3)}. \quad (17)$$

We can solve (16) for the $\hat{\Omega}\mathbf{e}_3$ term and independently project onto \mathbf{e}_1 and $-\mathbf{e}_2$ to determine the first two terms of Ω ,

$$\begin{bmatrix} \Omega_1 \\ \Omega_2 \end{bmatrix} = \begin{bmatrix} \mathbf{e}_1^T \\ -\mathbf{e}_2^T \end{bmatrix} R^T \frac{m}{f} \mathbf{x}^{(3)} \quad (18)$$

The third term of Ω is constrained by ψ . Consider

$$\Omega^{\mathcal{W}} = \begin{bmatrix} - \\ - \\ \dot{\psi} \end{bmatrix} = R\Omega \quad (19)$$

where $\Omega^{\mathcal{W}}$ is the angular velocity of the body expressed in the world coordinates. Then, Ω_3 can be determined using $\mathbf{e}_3^T R\Omega$

$$\Omega_3 = \frac{\dot{\psi} - \mathbf{e}_3^T (\mathbf{b}_1\Omega_1 + \mathbf{b}_2\Omega_2)}{\mathbf{e}_3^T \mathbf{b}_3} \quad (20)$$

Now we have introduced a singularity that is, to the best of our knowledge, unavoidable in the full 3-D case. Thus, any portion of the trajectory that passes through the singularity, we formulate as a vertical planar model, which results in a reduced-dimensional flat space with $\Omega_3 = 0$ as a constant when expressed in 3-D.

Another derivative of (2) provides

$$m\mathbf{x}^{(4)} = f \left(R\hat{\Omega}\mathbf{e}_3 + R\hat{\Omega}\hat{\Omega}\mathbf{e}_3 \right) + \dot{f}R\hat{\Omega}\mathbf{e}_3 + \ddot{f}\mathbf{b}_3 \quad (21)$$

and projecting onto \mathbf{b}_3 ,

$$\ddot{f} = m\mathbf{b}_3^T \mathbf{x}^{(4)} - f\mathbf{e}_3^T \hat{\Omega}^2 \mathbf{e}_3. \quad (22)$$

Similar to before, we can solve for the $\hat{\Omega}\mathbf{e}_3$ term and use the scalar projections onto \mathbf{e}_1 and $-\mathbf{e}_2$ to determine the first two elements of $\hat{\Omega}$. The third element can then be determined and will require the next derivative of ψ , $\ddot{\psi}$. Having the angular acceleration, we can solve for the required moments.

Thus, all the control inputs can be computed in terms of the *flat outputs* and their derivatives. Since the 4th derivative of position appears in the control inputs, we require that $\mathbf{x}(t) \in \mathcal{C}^4$. Similarly, the 2nd derivative of the yaw appears in the moments, which requires that $\psi \in \mathcal{C}^2$. From [22], the system is *differentially flat* and can be expressed as a chain of integrators in each of the flat outputs. When expressed in that form, the inputs to the system are $\mathbf{x}^{(4)}$ and $\ddot{\psi}$.

Physical and Sensor Constraints

There are a number of constraints that must be considered when planning aggressive trajectories. Since the trajectories are defined in the flat space, we need to transform the constraints to this specific space. First, the thrust is bounded by f_{max} . This condition can be expressed as

$$m \|\ddot{\mathbf{x}} + g\mathbf{e}_3\| \leq f_{max}. \quad (23)$$

The gyros saturate at ω_{max} , which imposes a bound on the jerk expressed from (18) with a β_1 function as

$$\beta_1(\mathbf{x}^{(3)}, \ddot{\mathbf{x}}, \dot{\psi}) \leq \omega_{max} \quad (24)$$

and the maximum moment along the i^{th} axis is bounded by $M_{i_{max}}$, requiring that

$$\beta_2(\mathbf{x}^{(4)}, \mathbf{x}^{(3)}, \ddot{\mathbf{x}}, \dot{\psi}, \psi) \leq M_{i_{max}}. \quad (25)$$

In practice, these constraints are coupled through (1). If the thrust is saturated, then all rotors are spinning at their maximum speed, and the moment inputs must be zero. Similarly, if a large moment is required, the thrust cannot simultaneously be zero. The thrust also cannot be zero because of the singularity in (11). For this reason, when planning, we further restrict certain constraints during portions of the trajectory that are expected to require large control inputs.

A Constrained Optimization Problem

The trajectories can be parametrized in each dimension using a basis function, $\mathbf{h}_i(t) \in \mathbb{R}^m$, and coefficients, $\mathbf{c}_i \in \mathbb{R}^m$, such that

$$\mathcal{Y}_i(t) = \mathbf{c}_i^T \mathbf{h}_i(t) \text{ for } i = 1, \dots, 4. \quad (26)$$

Next, an objective function is formulated to minimize the control inputs in the flat space. Minimizing the integral of the square of the n_i^{th} derivative of the i^{th} flat output provides the cost function,

$$\begin{aligned} \mathcal{J}_i &= \int_{t_0}^{t_f} \left\| \mathcal{Y}_i^{(n_i)}(t) \right\|^2 dt, \quad i = 1, \dots, 4 \\ &= \mathbf{c}_i^T \left[\int_{t_0}^{t_f} \mathbf{h}_i^{(n_i)}(t) \left[\mathbf{h}_i^{(n_i)}(t) \right]^T dt \right] \mathbf{c}_i \\ &\equiv \mathbf{c}_i^T H_i \mathbf{c}_i \end{aligned} \quad (27)$$

where $H_i \in \mathbb{R}^{m \times m}$ is used to formulate the problem as a Quadratic Program (QP):

$$\begin{aligned} &\text{minimize} && \mathbf{c}^T \mathcal{H} \mathbf{c} \\ &\text{subject to} && \mathbf{A} \mathbf{c} \leq \mathbf{B} \\ &&& \mathbf{A}_{eq} \mathbf{c} = \mathbf{B}_{eq} \end{aligned} \quad (28)$$

with

$$\mathbf{C} = \begin{bmatrix} \mathbf{c}_1 \\ \vdots \\ \mathbf{c}_4 \end{bmatrix}, \quad \mathcal{H} = \begin{bmatrix} H_1 & \mathbf{0} & \mathbf{0} \\ \mathbf{0} & \ddots & \mathbf{0} \\ \mathbf{0} & \mathbf{0} & H_4 \end{bmatrix},$$

with the constraints discussed in the previous section incorporated using a series of linear approximations in $\mathbf{A} \in \mathbb{R}^{k \times 4m}$ and $\mathbf{B} \in \mathbb{R}^k$ where k is the total number of linear constraints. The matrix $\mathbf{A}_{eq} \in \mathbb{R}^{p \times 4m}$ and vector $\mathbf{B}_{eq} \in \mathbb{R}^p$ can be used to impose p equality constraints. For example, we can use these to specify a velocity or acceleration constraint at a desired time.

The previous formulation is satisfactory for a single trajectory segment, but in practice, more than one segment is needed to maintain a high degree of freedom without resulting in computational errors. To keep the problem well conditioned, a desired trajectory is broken into segments with a maximum dt of 1 second. Then, the coefficients for each segment of a particular dimension can be stacked and incorporated into the QP. It is important to incorporate, as equality constraints, the requirement that the i^{th} dimension must be C^{n_i} , $n_i = 4, 4, 4, 2$.

We have tested three different numerical solvers including MATLAB's `quadprog` from the Optimization Toolbox and IBM's CPLEX¹, but have found Gurobi² to be the fastest and easiest to use.

Boundary Conditions

Now, we will discuss the specific boundary conditions to enable successful perching using our quadrotor. The initial conditions can be chosen to match the current state. It is assumed that the position and orientation (defined by a normal vector, \mathbf{n}) of the perch plate are known. Thus, the position at impact is defined such that the quadrotor would be perched on the window. The desired impact velocity can be determined from the landing envelope of the gripper. In addition, the tangential velocity is desired to be close to zero, but because of the design of the gripper, it is more important that if there is an error in the final velocity, it results in a downwards velocity. Thus, we aim for a slight downwards velocity when impacting the perch plate. A desired acceleration magnitude is not known, however, the vector \mathbf{b}_3 should be nearly aligned with \mathbf{n} or slightly pitched towards the plate so that the highest pad makes contact first and so that the plane of the quadrotor is parallel to the window.

From [16], we estimate that the time to change orientation by $\pi/2$ radians using our robots will be approximately 0.4 s. Thus, during the last portion of the trajectory (time dependent upon the orientation), we specify an acceleration such that \mathbf{b}_3 is parallel to

¹<http://www-01.ibm.com/software/commerce/optimization/cplex-optimizer/>
²www.gurobi.com

\mathbf{n} and the magnitude is such that the thrust is in the middle of its range to ensure that the robot has the moment control authority to rotate. It is important to consider gravity when imposing an acceleration constraint to specify an attitude. For example, if we would like the \mathbf{b}_3 vector to be at an angle θ and the thrust to be $f_{max}/2$, the acceleration must be expressed as

$$\dot{\mathbf{x}}^d = \begin{bmatrix} \frac{f_{max}}{2m} \sin(\theta) \\ 0 \\ \frac{f_{max}}{2m} \cos(\theta) - g \end{bmatrix}.$$

See Figure 8 and Figure 9 for a sample trajectory and acceleration vectors for a sample planar trajectory. See Figure 10 for the components of acceleration.

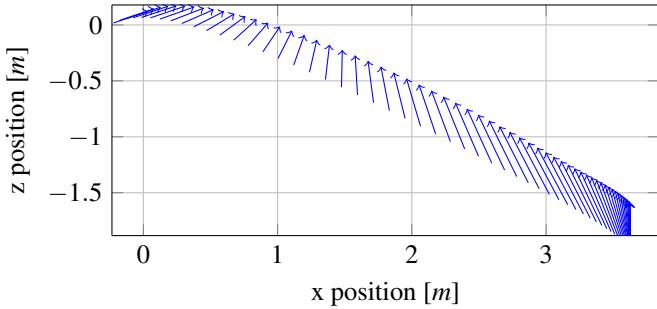


FIGURE 8. A sample trajectory with vectors denoting the acceleration (orientation and magnitude to scale). The quadrotor starts on the right and perches on the left at an incline of 70° . The box in the upper left corner is presented in a higher temporal resolution in Figure 9.

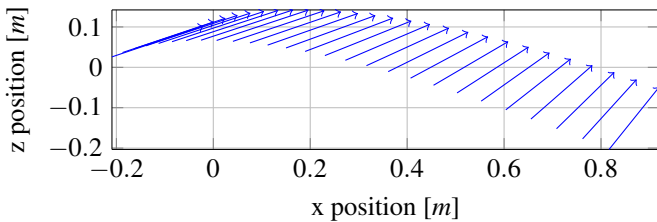


FIGURE 9. The last 40 ms of a sample perching trajectory. The arrows denote the acceleration direction (and direction of \mathbf{b}_3) and magnitude. Notice that the direction of the vector does not change significantly towards the end of the trajectory where the acceleration is bounded during planning.

Finally, it is expected that lower angular velocities during impact are more favorable. Thus, we impose constraints such that the angular rate is nearly zero.

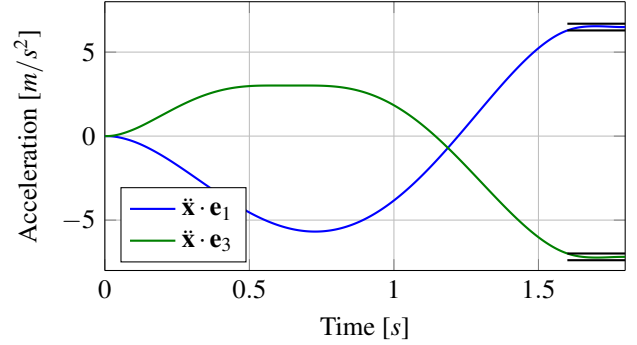


FIGURE 10. A plot of the nominal acceleration for the trajectory in Figure 8. Notice that during the last portion of the trajectory, the acceleration is bounded by the black lines, which dictates that the angular velocity will be nearly zero and that the robot will achieve the correct orientation before impact.

EXPERIMENTAL RESULTS

In this section, we present the experimental setup and the results of the perching trials. The experiments are conducted in the GRASP UAV Testbed [23] using a Hummingbird quadrotor made by Ascending Technologies³. A motion capture system is used for position feedback at 100 Hz. The setup is documented in Figure 11. Plots of various trajectories are provided in Figure 12 and of the angular velocities for 3 vertical surface perches in Figure 13. Successful perches on a vertical surface are denoted by yellow stars in Figure 4. Further, the reader is encouraged to view a video online⁴ to see successful perching.

Varying angles

Using the boundary conditions discussed in the previous section, we are able to vary the angle of the perch target without the need for iterative experimental trials (see Figure 12 for various orientations).

Surface Effects

During these experiments, we noticed the impact of aerodynamic surface effects as the robot became close to the perch plate. Even in quasi-static situations, surface effects are noticed [24]. Thus, this effect was not unexpected and was compensated by slightly increasing the desired impact velocity and decreasing the desired acceleration normal to the plate at impact. This resulted in a decreased thrust, and therefore, a decreased surface effect.

CONCLUSION AND FUTURE WORK

In this work, we presented a strategy for planning trajectories that enables quadrotors to perch on smooth surfaces while

³www.asctec.de

⁴http://youtu.be/P1t_cZqgsR8

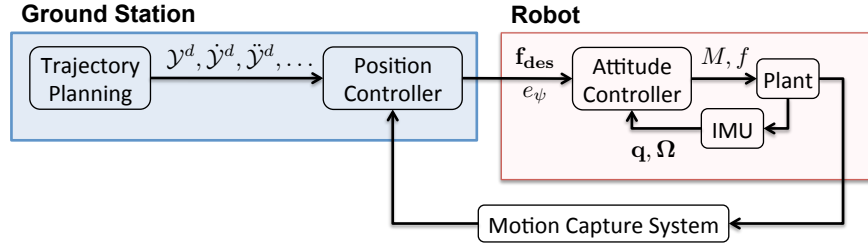


FIGURE 11. The architecture of the system. The ground station handles the trajectory planning and passes the trajectories to the position controller, which receives feedback from the motion capture system. The position controller sends a desired force, \mathbf{f}_{des} , a ψ error, and the necessary feedforward inputs to the robot. Internally, the attitude controller runs at 1 kHz to update the commanded force and moments based on the position controller’s command and the feedback from the IMU.

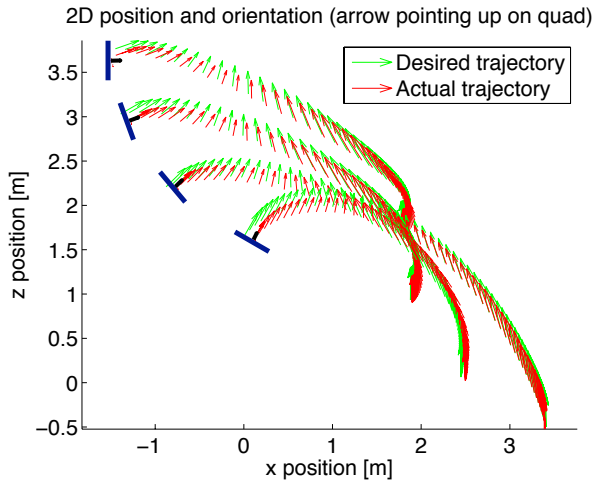


FIGURE 12. Using the proposed planning method, the angle of the surface can be changed without the need for iterative experimental trials. The root of each arrow indicates the position and the arrow indicates the direction of the thrust (*i.e.* the orientation of the robot).

taking into account constraints due to dynamics as well as limitations on actuators, sensors, and grippers. The approach can be extended to any aggressive maneuver. To show the effectiveness of the proposed methodology, we considered the perching of a quadrotor using a foot equipped with a dry-adhesive gripper on flat surfaces that can be inclined to the horizontal by as much as 90° . Future work will include perching on curved surfaces, bat-like perching by hanging, and sensing failures during perching. We will investigate the possibility to automate the gripper’s detaching process using an onboard actuator. Finally, we will explore vision-based techniques to enable perching without a dependence on an external motion capture system.

ACKNOWLEDGMENT

Thanks goes to Terry Kientz and Samer Nashed for their help in the design and mounting of the perch surface.

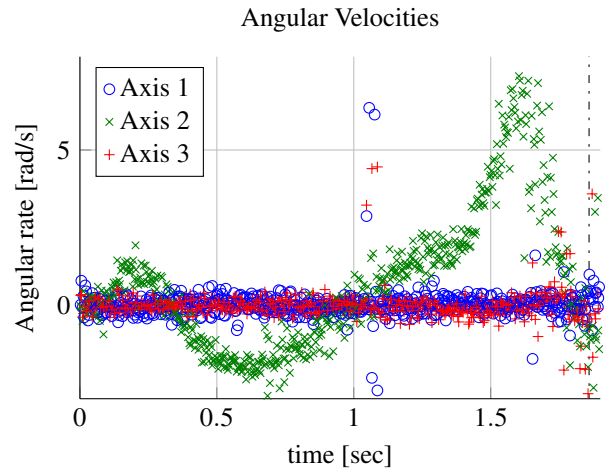


FIGURE 13. The angular velocities for 3 different perching trials on a vertical surface as estimated by the motion capture system. The vertical dash-dotted black line denotes the time of contact with the surface. As desired, the angular velocity is controlled to zero before impact.

We gratefully acknowledge support by ARL grant W911NF-08-2-0004, ONR grants N00014-07-1-0829, N00014-14-1-0510, N00014-09-1-1051, N00014-09-1-103, and NSF grants IIP-1113830, IIS-1426840, and IIS-1138847.

REFERENCES

- [1] Mulgaonkar, Y., Whitzer, M., Kroninger, C. M., and Aaron, M., 2014. “Power and Weight Considerations in Small, Agile, Quadrotors”. In Proc. SPIE 9083, Micro- and Nanotechnology Sensors, Systems, and Applications VI, Vol. 9083.
- [2] Lussier Desbiens, A., and Cutkosky, M. R., 2009. “Landing and Perching on Vertical Surfaces with Microspines for Small Unmanned Air Vehicles”. *Journal of Intelligent and Robotic Systems*, 57(1-4), Oct., pp. 313–327.

- [3] Kovač, M., Germann, J., Hürzeler, C., Siegwart, R. Y., and Floreano, D., 2010. “A perching mechanism for micro aerial vehicles”. *Journal of Micro-Nano Mechatronics*, 5(3-4), May, pp. 77–91.
- [4] Lussier Desbiens, A., Asbeck, A. T., and Cutkosky, M. R., 2011. “Landing, perching and taking off from vertical surfaces”. *The International Journal of Robotics Research*, 30(3), Jan., pp. 355–370.
- [5] Moore, J., and Tedrake, R., 2009. “Powerline Perching with a Fixed-Wing UAV”. *AIAA Infotech@Aerospace Conference*, Apr., pp. 1–16.
- [6] Moore, J., Cory, R., and Tedrake, R., 2014. “Robust post-stall perching with a simple fixed-wing glider using LQR-Trees.”. *Bioinspiration & Biomimetics*, 9, p. 025013.
- [7] Doyle, C. E., Bird, J. J., Isom, T. A., Johnson, C. J., Kallman, J. C., Simpson, J. A., King, R. J., Abbott, J. J., and Minor, M. A., 2011. “Avian-inspired passive perching mechanism for robotic rotorcraft”. In 2011 IEEE/RSJ International Conference on Intelligent Robots and Systems, IEEE, pp. 4975–4980.
- [8] Doyle, C. E., Bird, J. J., Isom, T. a., Kallman, J. C., Bareiss, D. F., Dunlop, D. J., King, R. J., Abbott, J. J., and Minor, M. a., 2013. “An avian-inspired passive mechanism for quadrotor perching”. *IEEE/ASME Transactions on Mechatronics*, 18(2), pp. 506–517.
- [9] Chi, W., Low, K. H., Hoon, K. H., and Tang, J., 2014. “An Optimized Perching Mechanism for Autonomous Perching with a Quadrotor”. In International Conference on Robotics & Automation (ICRA), IEEE, pp. 3109–3115.
- [10] Hawkes, E. W., Christensen, D. L., Eason, E. V., Estrada, M. A., Heverly, M., Hilgemann, E., Jiang, H., Pope, M. T., Parness, A., and Cutkosky, M. R., 2013. “Dynamic surface grasping with directional adhesion”. In International Conference on Intelligent Robots and Systems (IROS), IEEE, pp. 5487–5493.
- [11] Daler, L., Klaptocz, A., Briod, A., Sitti, M., and Floreano, D., 2013. “A perching mechanism for flying robots using a fibre-based adhesive”. In International Conference on Robotics and Automation (ICRA), IEEE, pp. 4433–4438.
- [12] Jiang, H., Pope, M. T., Hawkes, E. W., Christensen, D. L., Estrada, M. A., Parlier, A., Tran, R., and Cutkosky, M. R., 2014. “Modeling the Dynamics of Perching with Opposed-Grip Mechanisms”. In International Conference on Robotics and Automation (ICRA), IEEE.
- [13] Zhang, Z., Xie, P., and Ma, O., 2013. “Bio-inspired trajectory generation for UAV perching”. In IEEE/ASME International Conference on Advanced Intelligent Mechatronics (AIM), IEEE, pp. 997–1002.
- [14] Mellinger, D., Michael, N., and Kumar, V., 2010. “Trajectory Generation and Control for Precise Aggressive Maneuvers with Quadrotors”. In International Symposium on Experimental Robotics (ISER).
- [15] Mellinger, D., Shomin, M., and Kumar, V., 2010. “Control of Quadrotors for Robust Perching and Landing”. In International Powered Lift Conference (IPLC).
- [16] Mellinger, D., Michael, N., and Kumar, V., 2012. “Trajectory generation and control for precise aggressive maneuvers with quadrotors”. *The International Journal of Robotics Research (IJRR)*, 31(5), Jan., pp. 664–674.
- [17] Mohta, K., Kumar, V., and Daniilidis, K., 2014. “Vision-based Control of a Quadrotor for Perching on Lines”. In International Conference on Robotics and Automation (ICRA), IEEE.
- [18] Thomas, J., Polin, J., Sreenath, K., and Kumar, V., 2013. “Avian-Inspired Grasping for Quadrotor Micro UAVs”. In International Design Engineering Technical Conferences & Computers and Information in Engineering Conference (IDETC/CIE), ASME.
- [19] Lee, T., Leok, M., and McClamroch, N. H., 2010. “Geometric tracking control of a quadrotor UAV on SE(3)”. In 49th IEEE Conference on Decision and Control (CDC), no. 3, IEEE, pp. 5420–5425.
- [20] Mellinger, D., and Kumar, V., 2011. “Minimum snap trajectory generation and control for quadrotors”. In International Conference on Robotics and Automation (ICRA), IEEE, pp. 2520–2525.
- [21] Fliess, M., Lévine, J., Martin, P., and Rouchon, P., 1995. “Flatness and defect of non-linear systems: introductory theory and examples”. *International Journal of Control*, 61(6), June, pp. 1327–1361.
- [22] Murray, R., Rathinam, M., and Sluis, W., 1995. “Differential flatness of mechanical control systems: A catalog of prototype systems”. In ASME International Congress and Exposition, Citeseer.
- [23] Michael, N., Mellinger, D., Lindsey, Q., and Kumar, V., 2010. “The GRASP Multiple Micro-UAV Testbed”. *IEEE Robotics & Automation Magazine*, 17(3), Sept., pp. 56–65.
- [24] Powers, C., Mellinger, D., Kushleyev, A., Kothmann, B., and Kumar, V., 2012. “Influence of Aerodynamics and Proximity Effects in Quadrotor Flight”. In Proceedings of the International Symposium on Experimental Robotics (ISER).